Second Conference on Smart Monitoring,
Assessment and Rehabilitation of Civil Structures

SMAR 2013

Recent developments in optical systems for structural deflection measurement

Derek D. Lichti[1], Ayman F. Habib[1], Mamdouh El-Badry[2], Ivan Detchev[1] and Xiaojuan Qi[1]

[1] Department of Geomatics Engineering, The University of Calgary, Calgary, Canada
[2] Department of Civil Engineering, The University of Calgary, Calgary, Canada

ABSTRACT: This paper reports recent developments of optical imaging systems for the measurement of structural deflections from fatigue loading. Two imaging systems developed at the University of Calgary are described, one based on active range camera technology and the other on passive digital cameras. The salient characteristics of each, including the hardware components, data quality and data processing methods, are described. Results are presented from the measurement of a reinforced concrete beam subjected to fatigue loading at 1 Hz and 3 Hz. Comparison of the results with those from laser displacement sensors shows that both imaging systems can achieve sub-millimeter accuracy in terms of the displacement amplitude.

1 INTRODUCTION

Civil infrastructure systems in Canada and many other nations are deteriorating at an alarming rate due to inadequate maintenance, excessive loading, economically-driven design practices, and adverse environmental conditions. Structural health monitoring of crucial infrastructure such as bridges is therefore important for ensuring both safety and serviceability over their lifespan. Safety refers to the ability of a structure to withstand without failure the maximum loads estimated during the design stage, whereas serviceability refers to a satisfactory performance of the structure over its service life. Excessive deformations, particularly deflection under repeated moving loads (e.g. due to traffic) are one of the main factors that can adversely affect serviceability of a structure. A viable solution to enhance performance and extend the service life of concrete bridges is to bond fibre- or steel-reinforced polymer sheets to the surface of structural elements such as beams and girders. Prior to application of these sheets in situ, their efficacy must be assessed through controlled laboratory testing in which deflection of strengthened beam or girder specimens is measured under static monotonic and cyclic fatigue loading.

Traditional methods of deflection measurement include contact sensors such as dial gauges and linear variable differential transformers (LVDTs) and non-contact laser displacement sensors (LDSs). Whilst all these offer very high precision (up to 2 μm), they suffer from several drawbacks: collection of only one-dimensional data; limited measurement range; large expense to deploy many sensors across an entire structure; and high potential for destruction during testing. Optical techniques based on digital photogrammetry (Barazzetti and Scaioni, 2010; Fraser and Riedel, 2000; Maas and Hampel, 2006) and laser scanning (Gordon and Lichti, 2007; Park et al., 2007; Rönnholm et al., 2009) have been shown to be very effective and accurate for static load test measurements. The relatively recent development of range cameras has, however, opened the possibility of dynamic load test measurements.

This paper describes new developments in the measurement of deflections during fatigue load testing with two different systems developed at the University of Calgary: one based on range camera technology and the other based on a digital photogrammetric system. First, the basic principles of each measurement technique are briefly reviewed. Next, the new innovations in terms of measurement system deployment and data processing algorithms are described. These are followed by the description of a fatigue load testing experiment conducted in the University structures laboratory. The experimental results and analyses are followed by the conclusions.

2 OPTICAL MEASUREMENT TECHNIQUES

2.1 Range imaging

A range camera (Figure 1) is a solid-state active imaging device that measures range at each pixel. The camera's integrated light emitting diodes emit a cone of amplitude-modulated near-infrared light that illuminates the scene to be measured. The reflected light is focused by the lens onto a solid-state sensor. The received signal is demodulated at each pixel location to obtain the phase difference between it and the emitted signal, which is scaled to obtain the range. Lange and Seitz (2001) give a more complete description of the measurement process. The output of the camera comprises co-located range and amplitude images (Figure 1) and derived three-dimensional (3D) co-ordinates, which are calculated by scaling the fundamental collinearity equations of photogrammetry (e.g., Lichti et al., 2012). The largest array size of commercially-available range camera systems is approximately 40,000 pixels^2, though the Mesa SwissRanger SR4000 used herein features just over 25,000 (176 x 144) pixels^2. The maximum unambiguous range, which is governed by the modulation frequency, is generally less than 10 m, so a range camera is best suited to close-range applications. Measurement precision is typically specified to be in the order of a few millimeters. The SR4000 manufacturer's accuracy specification is 10 mm or 1% of the object distance, whichever is greater. Piatti and Rinaudo (2012) give a comprehensive review of available systems.

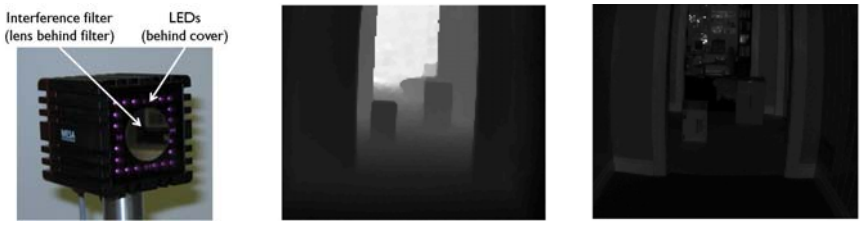

Figure 1. The SR4000 range camera (left). Range image of hall scene (center). Amplitude image (right).

Range cameras are highly attractive for structural measurement due their compact, hand-held size, low cost (~€3000) and ability to capture 3D data time series at a rate of up to 50 Hz in the SR4000 case. It has been demonstrated that range cameras are capable of measuring static deflections with millimeter accuracy (Lichti et al., 2012) and their potential for dynamic measurement is very high.

Range camera data are corrupted by numerous random and systematic error sources that degrade their accuracy. Several quality assurance processes therefore need to be followed to mitigate the errors as much as possible. These include camera calibration to determine instrumental systematic errors that can be readily modeled such as lens distortions and periodic range errors (Lichti et al., 2010). The influence of shot noise, the limiting random error source in range imaging, can be reduced through temporal and spatial averaging of acquired data (Lindner et al., 2010) if the measurement regime permits (i.e., static scenes of object that can be

readily modeled) as well as careful selection of certain camera parameters such as the integration time and the modulation frequency. Other range errors can be reduced through best practice procedures. Camera warm-up times of 40-60 min have been suggested to allow transient range errors to decay (e.g., Chiabrando et al., 2009). Range errors that depend on the structure of the scene being measured are difficult to model but, fortunately, can be largely eliminated when differential measurements such as deflections are required (Lichti et al., 2012).

The data capture process with a range camera is relatively straightforward thanks to demonstrator software and development libraries provided by the manufacturers. However, the application of range cameras to a particular measurement task requires purpose-built software to recognize and extract objects of interest from the noisy data. This can involve a variety of image processing algorithms applied to the range and amplitude imagery and the 3D point cloud.

2.2 Photogrammetric system

Photogrammetry is the inverse process of photography. In photography a camera is used to capture a three-dimensional (3D) scene onto a two-dimensional (2D) medium, nowadays usually a solid sensor. In photogrammetry, multiple 2D images acquired from different locations and orientations are used to perform the 3D reconstruction of the original scene. Since a traditional digital camera is a passive imaging device and measures only the intensity (and not the range) for each pixel location, a minimum of two camera stations are needed for the 3D reconstruction. The typical example of photogrammetric reconstruction is the stereo photography scenario in Figure 2. In this example, conjugate points are identified in the left and right images, and by knowing the locations of the two perspective centers (PCs) and the orientation of the two light rays, the position of the point of interest is intersected in the object space. This reconstruction principle uses the collinearity condition, which states that each set of homologous image and object points plus their corresponding perspective center all lie on a straight line (Kraus, 1993).

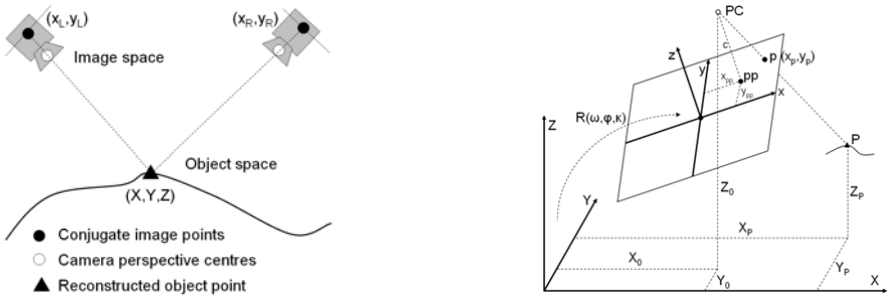

Figure 2. a) Traditional stereo photography setup. b) The principle of the collinearity equations.

In order to aid the process of identifying conjugate points in overlapping images, a random pattern can be projected onto the scene to create artificial texture on a surface that could otherwise be homogeneous, such as a concrete beam. This is especially helpful when a full surface reconstruction is necessary and placing numerous physical markers or targets is either not feasible or undesirable (Reiss and Tommaselli, 2011).

The precision of the final reconstruction outcome depends on many factors such as the number of camera stations, their network geometry, the pixel measurement accuracy, and the system calibration. The system calibration can be divided into two procedures. One of them estimates the interior orientation parameters (IOPs) of the camera, and is known as camera calibration (Habib and Morgan, 2003). The other one estimates the exterior orientation parameters (EOPs) of each image/camera station. The IOPs consist of the principal point coordinates (i.e., the projection of the PC on the image plane), the principal distance (i.e., the distance between the PC and the

principal point; Figure 2), and some additional parameters such as lens distortion coefficients, which describe any deviations from the collinearity condition. The EOPs include the position of the PC and the orientation of the image coordinate system for each camera station with respect to the object space reference frame. The position is defined by a 3D vector in Cartesian space, and the orientation is defined by three rotation angles (see Figure 2). In addition to performing a camera calibration procedure, the camera(s) should be subjected to a stability analysis procedure to verify that the IOPs do not change over time since off-the-shelf digital cameras are not designed specifically for metric applications such as structural measurement (Habib and Morgan, 2005).

The identification of conjugate points in two or more images is one of the greatest challenges in photogrammetry. It is a very time consuming and mundane process. Therefore, automatic methods are preferred to manual measurement. The former usually require a corner detector, such as the Harris operator (Harris and Stephens, 1988), and a matching algorithm such as normalized cross correlation (e.g., Schenk, 1999). Several geometric constraints can be imposed to reduce the search space for each image pair and thereby decrease the processing time and matching reliability (Detchev et al., 2011).

3 EXPERIMENT DESCRIPTION

3.1 Test subject and setup

Fatigue load testing was performed on a 3 m long, white-washed reinforced concrete beam having a 150 mm x 300 mm rectangular cross section (Figure 3). A hydraulic actuator was used to apply periodically-varying two-point load on the beam via a spreader beam. The system for measuring the concrete beam displacement comprised a target system and the measurement devices. Since most of the top surface of the concrete beam was occluded by the spreader beam, the target system comprised thirteen white-washed, thin aluminum plates (220 mm x 50 mm) bonded to the side of the beam at an interval of 250 mm along its length. Three measurement systems were used: a range camera system comprising two SwissRanger SR4000 devices; an eight-camera and a two-projector digital photogrammetric system; and five KEYENCE LK-G407 CCD LDSs. The optical sensors were rigidly mounted to a scaffold frame approximately 2.0 m above the top of the concrete beam. The LDSs were mounted beneath several of the thin aluminum plates.

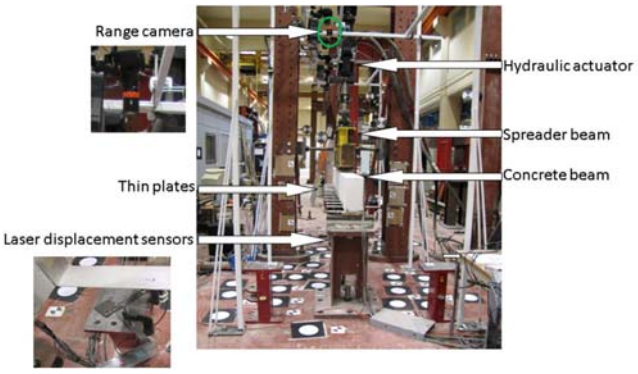

Figure 3. The fatigue load testing and measurement setup.

3.2 Loading regime

Before the fatigue loading test was performed, a static loading regime based on displacement control and force control was executed in four steps. First, displacement-controlled static

loading was applied with a 3 mm stroke at a rate of 1 mm/min. Second, the concrete beam was unloaded to zero displacement at the same rate. Third, the 3 mm stroke was applied again at the same rate. Fourth, the concrete beam was unloaded at the same rate. Next, force-controlled loading was executed. The periodic load was first applied to the beam at 1 Hz then at 3 Hz. Over 36000 load cycles were applied from 24 kN to 96 kN causing 4 mm displacement amplitude (8 mm peak-to-peak displacement).

3.3 Data capture

Several quality assurance measures were followed for the range camera data capture. First, the 3D range cameras were warmed up for one hour to obtain stable measurement data. Second, the two cameras' modulation frequencies were set to 31 MHz (Camera 1) and 29 MHz (Camera 2) to prevent data biases due to light interference. Several 5 s long datasets were captured with different sampling frequencies by varying the integration time in order to test the range cameras' capabilities. Values of 21 ms, 8.5 ms, 4.4 ms and 2.2 ms were used, for which the respective sampling frequencies were 10 Hz, 20 Hz, 30 Hz and 40 Hz.

The photogrammetric system included two groups of four cameras and one projector each. Each group of devices was placed symmetrically on each side of the beam. Canon EOS 1000D digital single-lens reflex cameras with a 22.2 x 14.8 mm^2 complementary metal oxide semiconductor (CMOS) solid state sensor were used. The output images had a maximum resolution of 10.1 $Mpixel^2$ with a pixel size of 5.71 μm. According to manufacturer specifications, the cameras support continuous shooting of up to three frames per second (Canon Inc., 2008). The cameras were synchronized to 5 ms through a remote control connected to a hub, which could split the shutter release signal to all eight cameras. Single-chip digital light processing projectors (BenQ MP522 ST) were used. These are short-throw projectors with an extended graphics array (XGA) and a resolution of 1024 x 768 $pixel^2$ (BenQ Corp., 2008). With camera and projector costs of $450 and $750, the overall system cost was approximately $5,100, excluding cables, the computer used for data storage and the development of the in-house software.

Data captured with the KEYENCE LDSs served as the basis against which the performance of the other two systems could be benchmarked. The high quality of this sensor (linearity: 0.05% of the ±100 mm measurement range; 2 μm precision) and 300 Hz sampling rate allowed the LDSs to serve as a reliable reference. LDS data capture was performed concurrently with the other sensors so that results could be directly compared.

4 EXPERIMENT RESULTS

4.1 Range camera

The aim of the range camera data processing was to reconstruct the trajectory of the thin plate targets from the time series of range camera data. The targets were extracted from each frame of the time series according to the following process. The first step was depth-based segmentation based on the range data, which yielded a binary image of blobs representing the thin plates. Since the range cameras were nadir-looking and the beam was horizontal, all thin plates were positioned at the same height in the camera's internal co-ordinate system. Since the blobs contained erroneous points due to measurement artifacts, principally mixed pixels (Lichti et al., 2012), they were refined by eccentricity analysis and image morphology. Figure 4 shows the input and output of the process. The final step was computation of the centroid of each blob.

The time-domain signal of each target's trajectory was then reconstructed from the time series of blob centroids with a semi-automatic process. First, the mean of the time series was

computed and subtracted prior to spectral analysis. Second, the nominal loading frequency was identified from the magnitude spectrum. The third step was initial signal reconstruction by linear least squares to estimate the amplitude and phase using the nominal loading frequency. The fourth step was the final signal reconstruction by non-linear least squares to estimate the amplitude, the phase, the frequency and the signal mean.

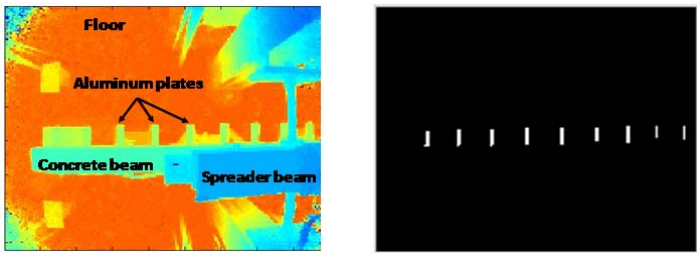

Figure 4. Range image (left) and extracted thin plate blobs (right).

Although the range camera is a 3D measurement system, only the vertical component of the target measurement is reported here since deflections were of primary interest in the fatigue load testing. Results are presented for the aluminum plate located at the beam's mid-span where the deflection was the greatest. Aliasing of the measured signal was not a problem thanks to the high frame rate of the camera in relation to the loading frequency. Results from 3 Hz load testing are presented in Figure 5 for two different range camera sampling frequencies (f_s). In both cases the reconstructed signal fits the data but the increase in noise level is clear as the sampling frequency increases and, therefore, the integration time decreases. This is reflected statistically by the standard deviations of the least-squares residuals (σ). A summary of the estimated signal parameters of interest, the amplitude (A) and loading frequency (f_0) is given for the same thin plate and the two cameras in Table 1. The high accuracy of both cameras is apparent when these results are compared to the reference values determined from the LDS data: f_0=3.0843 Hz and A=4.00 mm. The sub-millimeter accuracy estimates of the amplitude are particularly impressive when it is recalled that the range camera's accuracy specification is 10 mm.

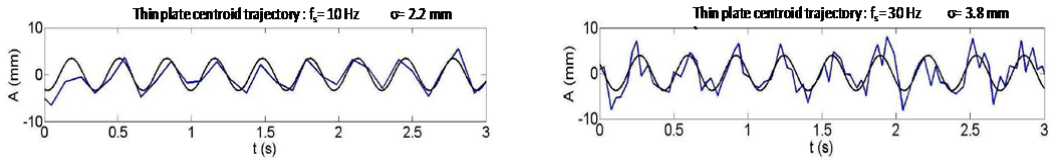

Figure 5. Range camera target centroid raw data (blue) and reconstructed trajectory (black) for two different sampling rates (10, 20, 30 and 40 Hz), 3 Hz loading frequency and 4 mm amplitude.

4.2 Photogrammetric system

After the photogrammetric reconstruction was done, a segmentation-based algorithm was applied for the extraction and identification of the thin plates. The centroid was computed from the reconstructed points on each of the thin plates. The vertical deflection of the beam could then be estimated by tracking the Z-coordinates of the plate centroids over time. The static repeatability for the vertical deflections (δZ) of five sets of data during the zero load epoch (i.e., before the actual experiment started) had a root mean square error (RMSE) of 0.05 mm.

Table 1. Central thin plate amplitudes and loading frequencies estimated from the range camera data.

f_s (Hz)	Camera 1 A (mm)	Camera 2 A (mm)	Camera 1 f_0 (Hz)	Camera 2 f_0 (Hz)
10	3.42	3.50	3.0846	3.0841
20	3.80	3.64	3.0834	3.0840
30	3.86	4.51	3.0853	3.0840
40	4.07	4.71	3.0904	3.0845

Since during the dynamic loading phase of the experiment the concrete beam was repeatedly subjected to the same load range, the vertical displacement of the thin plates exhibited a cyclic motion. The amplitude of this vertical motion was derived using the photogrammetric system. The methodology for estimating the amplitude was very similar to the one described for the range camera. The dynamic repeatability for the differences in the estimated vertical motion amplitude (ΔA) for three sets of data during the 1 Hz dynamic loading phase of the experiment had an RMSE of 0.03 mm. In this case, a value representing the loading frequency could also be estimated. However, since precise time stamps were not available from the cameras, the recovered frequency value was not the true loading frequency. Thus, this estimated loading frequency was treated as a nuisance parameter similar to the phase and the mean value of the vertical motion signal, and was not reported here. The derived amplitudes by the photogrammetric system were compared to the derived amplitudes from the control LDS at the central plate. As seen from Table 2, the difference in the estimated amplitudes by the two systems was 0.07 mm.

Table 2. Estimated amplitudes by the LDS and the photogrammetric system at the central thin plate for the 1 Hz dynamic loading phase of the experiment.

Approximate Time	LDS A (mm)	Photogrammetric System A (mm)
2:39 pm	3.89	–
2:41 pm	–	3.82
2:46 pm	–	3.82
2:49 pm	3.90	–
2:58 pm	3.91	–
3:03 pm	–	3.84
3:08 pm	3.91	–
Mean	3.90	3.83

5 CONCLUSIONS

Two optical imaging systems recently developed for the measurement of structural deflections from fatigue loading have been described. The first is based on range camera technology and the second based on high-resolution, passive digital cameras. Results from fatigue load testing of a reinforced concrete beam have demonstrated that both are capable of measuring deflection as a function of time with sub-millimeter accuracy. In each case, the design of the data processing algorithms and the quality assurance measures are critical factors in achieving these results. The implication of the outcomes is that dynamic vertical displacement measurements of structures can be achieved remotely in a laboratory setting with relatively low-cost components.

6 ACKNOWLEDGEMENTS

This research is supported by the Natural Sciences and Engineering Research Council (NSERC) of Canada.

7 REFERENCES

Barazzetti, L and Scaioni, M. 2010. Development and implementation of image-based algorithms for measurement of deformations in material testing, *Sensors*, 10 (8): 7469-7495.

BenQ Corp., 2008. BenQ MP512 ST / MP522 ST Digital Projector User Manual.

Canon Inc., 2008. EOS Rebel XS / EOS 1000D Instruction Manual.

Chiabrando, F, Chiabrando, R, Piatti, D and Rinaudo, F. 2009. Sensors for 3D imaging: metric evaluation and calibration of a CCD/CMOS time-of-flight camera. *Sensors,* 9 (12): 10080-10096.

Detchev, I., Habib, A., Chang, Y.-C., 2011. Image matching and surface registration for 3D reconstruction of a scoliotic torso. *Geomatica* 65, 175–187.

Fraser, CS and Riedel, B. 2000. Monitoring the thermal deformation of steel beams via vision metrology." *ISPRS Journal of Photogrammetry and Remote Sensing*, 55 (1): 268-276.

Gordon, SJ and Lichti, DD. 2007. Modeling terrestrial laser scanner data for precise structural deformation measurement. *ASCE Journal of Surveying Engineering*, 133 (2): 72-80.

Habib, AF, Morgan, MF, 2003. Automatic calibration of low-cost digital cameras. *Optical Engineering* 42, 948–955.

Habib, AF, Morgan, MF, 2005. Stability analysis and geometric calibration of off-the-shelf digital cameras. *Photogrammetric Engineering & Remote Sensing* 71, 733–741.

Harris, C, Stephens, M. 1988. A combined corner and edge detector. Presented at the 4th Alvey Vision Conference, Manchester, UK, pp. 147–151.

Kraus, K. 1993. *Photogrammetry*, *Volume 1: Fundamentals and Standard Processes*. Ferd. Duemmlers Verlag, Bonn.

Lange, R, and Seitz, P. 2001. Solid-state time-of-flight range camera. *IEEE Journal of Quantum Electronics,* 37 (3): 390-397.

Lichti, DD, Kim, C and Jamtsho, S. 2010. An integrated bundle adjustment approach to range-camera geometric self-calibration. *ISPRS Journal of Photogrammetry and Remote Sensing*, 65 (4): 360-368.

Lichti, DD, Jamtsho, S, El-Halawany, SI, Lahamy, H, Chow, J, Chan, TO and El-Badry, M. 2012. Structural deflection measurement with a range camera. *ASCE Journal of Surveying Engineering*, 138 (2): 66-76.

Lindner, M, Schiller, I, Kolb, A and Koch R. 2010. Time-of-flight sensor calibration for accurate range sensing. *Computer Vision and Image Understanding*, 114 (12): 1318-1328.

Maas, H-G and Hampel, U. 2006. Photogrammetric techniques in civil engineering material testing and structure monitoring, *Photogrammetric Engineering & Remote Sensing*, 72 (1): 39–45.

Park, HS, Lee, HM, Adeli, H and Lee, I. 2007. A new approach for health monitoring of structures-terrestrial laser scanning, Computer Aided Civil Infrastructure Engineering, 22 (1): 19-30.

Piatti, D and Rinaudo, F. 2012. SR-4000 and CamCube3.0 time of flight (ToF) cameras: tests and comparison. *Remote Sensing*, 4 (4): 1069-1089.

Reiss, MLL and Tommaselli, AMG. 2011. A low-cost 3D reconstruction system using a single-shot projection of a pattern matrix. *The Photogrammetric Record* 26, 91–110.

Rönnholm, P, Nuikka, M, Suominen, A, Salo, P, Hyyppä, H, Pöntinen, P, Haggrén, H, Vermeer, M, Puttonen, J, Hirsi, H, Kukko, A, Kaartinen, H, Hyyppä, J and Jaakkola, A. 2009. Comparison of measurement techniques and static theory applied to concrete beam deformation. *Photogrammetric Record*, 24 (128) 351-371.

Schenk, T. 1999. *Digital Photogrammetry*. TerraScience, Laurelville, Ohio.